GENERATION OF NEARSHORE OBLIQUE SAND BARS: SENSITIVITY TO SAND TRANSPORT FORMULATION

F. RIBAS, N.C. VIS-STAR AND H.E. DE SWART

Institute for Marine and Atmospheric research Utrecht, Utrecht University, Princetonplein 5, 3584CC Utrecht, The Netherlands, E-mail: f.ribas@phys.uu.nl

A. FALQUÉS

Applied Physics Department, Universitat Politècnica de Catalunya, Jordi Girona 1-3, 08034 Barcelona, Spain, E-mail: falques@fa.upc.es

A model is analysed that describes the initial formation of nearshore oblique bars as a result of inherent instabilities in the coupling between the wave-driven nearshore circulation and the erodible bottom. The aim is to gain fundamental knowledge about the sensitivity of bar generation to the formulation for sand transport. Three well-known transport formulas (Bailard bedload, Bailard suspended load and Engelund-Hansen total load) have been used in the limit of weak currents compared to wave orbital velocities. The differences in the cross-shore distribution of their wave stirring functions results in different characteristics of the fastest growing modes. Results are also sensitive to the angle between the net sediment transport and the net current: anisotropic transport causes bar shapes to change and growth rates to increase substantially.

1. Introduction

Patches of nearshore oblique sand bars are sometimes observed in the nearshore zone of coastal seas. These bars have elongated crests oriented at a certain angle with respect to the coastline. They mainly emerge during periods of obliquely incident waves, which drive longshore currents. Spacings between successive crests range from tens to hundreds of meters and typical migration celerities can be of the order of meters per day in the direction of the current (see Ref. 4 for field observations). As the presence or absence of these bars affect coastal stability it is important to gain fundamental knowledge about their dynamics.

The emergence of nearshore rhythmic bars has often been related to the sediment transport induced by standing low-frequency edge waves [6]. An alternative explanation for their generation is based on the concept of

morphodynamical self-organization. Coupling between topographic perturbations superimposed on an alongshore uniform beach profile and the resulting hydrodynamic perturbations can lead to convergence of sand transport over the bars, hence producing a positive feedback. Linear stability analysis (LSA) is a convenient tool to investigate this possible feedback, yielding information about the shape, growth rate and migration celerity of the initially emerging modes. It also allows for a systematic exploration of the sensitivity of bar dynamics to the formulation of different physical processes.

In recent studies, LSA has been employed to investigate the generation of nearshore oblique bars on planar reference beach profiles (Refs. 1 and 6). They demonstrate that self-organization can exist and that the computed topographic patterns resemble those of observed oblique bars. The existence of persistent obliquely incident waves is crucial for the formation of these bars. A systematic exploration of the sensitivity of bar characteristics to different physical conditions was examined in Ref. 6. The highly idealized model used there contains a sand transport proportional to a specific power of the depth- and wave-averaged current. It was found that the shape and dynamics of the emerging bars strongly depend on the specific formulation of the sediment transport.

Motivated by these results, the present contribution aims at further exploring the sensitivity of bar characteristics to more realistic sediment transport formulations, in case of wave-dominated conditions and planar reference profiles. Therefore, the dynamical equations presented in Ref. 6 have been used. They are briefly presented in section 2. Section 3 describes the method used to perform the linear stability analysis. The results, presented in section 4, show the dependence of bar characteristics on differences in the cross-shore distributions of the wave stirring and in the angle between the net sediment transport and the net current (anisotropic transport). Section 5 gives a physical interpretation of the results and the conclusions are listed in section 6.

2. Model formulation

The model used in this study describes feedbacks between mean currents, waves and an erodible bed in a nearshore zone bounded by a straight coast. The alongshore averaged beach profile is assumed to be planar (no shore-parallel bars). The y-axis is chosen to coincide with the coastline, x-axis and z-axis point in the seaward and upward directions, respectively. Fluid

motions are based on the wave and depth-averaged momentum and mass conservation equations,

$$\frac{\partial v_i}{\partial t} + v_j \frac{\partial v_i}{\partial x_j} = -g\frac{\partial z_s}{\partial x_i} - \frac{\tau_{bi}}{\rho D} - \frac{1}{\rho D}\frac{\partial \mathcal{S}'_{ij}}{\partial x_j} + \frac{1}{\rho D}\frac{\partial \mathcal{S}''_{ij}}{\partial x_j} , \quad i = 1,2 \qquad (1)$$

$$\frac{\partial D}{\partial t} + \frac{\partial (D v_j)}{\partial x_j} = 0 . \qquad (2)$$

Here, $\vec{v} = (v_1, v_2)$ is the wave- and depth-averaged horizontal velocity, $x_1 = x$, $x_2 = y$ and repeated indexes are assumed to be summed. Furthermore, g is the acceleration due to gravity, ρ is the water density, z_s is the mean free surface elevation and $D = z_s - z_b$ is the total depth, where the sea bottom level is defined by $z = z_b$. The bed shear stresses in the x- and y-direction are described by τ_{b1} and τ_{b2}, respectively. The wave radiation stresses are denoted by $\mathcal{S}'_{ij}$ and $\mathcal{S}''_{ij}$ are the Reynolds turbulent stresses.

To close the hydrodynamical model, explicit formulations of the stresses $\mathcal{S}'_{ij}$, τ_{bi} and $\mathcal{S}''_{ij}$ are needed. This study focuses on the fundamental physical mechanisms that can lead to bar formation (*'bottom-up approach'*) and this motivates the following simplifications regarding the description of waves: (a) shallow water kinematics, (b) small angle of wave incidence with respect to shore-normal, (c) regular monochromatic waves, (d) saturated waves inside the surf zone, $H = \gamma_b D$ (where $\gamma_b \simeq 0.8$ is a constant), and (e) no wave forcing out of the surf zone, $H = \text{const}$. Details of these assumptions can be found in Refs. 5 and 6. Furthermore, only refraction of waves due to the depth-varying alongshore-uniform beach profile is considered (using Snell's law). Finally, the net currents are assumed to be weak with respect to the wave orbital velocity amplitudes (weak current limit) and the effects of currents on wave propagation are neglected. Consequently, the wave radiation stresses read

$$\mathcal{S}'_{11} = \frac{3}{2}E , \quad \mathcal{S}'_{22} = \frac{1}{2}E , \quad \mathcal{S}'_{12} = -E\sqrt{\frac{H}{H_b}}\,\sin\theta_b .$$

Here, $E = \frac{1}{8}\rho g H^2$ is the energy density of waves, whilst H_b and θ_b are the wave height and the angle of wave incidence at the breaker line. Bed shear stresses are parameterized as being proportional to the mean flow. They are the first order approximations of the stresses described by the standard quadratic friction law, in the case of weak current limit,

$$\tau_{b1} = \frac{4}{\pi}\rho\, c_d\, u_w\, v_1 , \quad \tau_{b2} = \frac{2}{\pi}\rho\, c_d\, u_w\, v_2 , \quad \text{with} \quad u_w = \frac{H}{2}\sqrt{\frac{g}{D}} .$$

They include a drag coefficient, c_d (assumed to be constant) and the amplitude of the wave orbital velocity near the bed, u_w (which follows from linear wave theory). The turbulent Reynolds stresses, $\mathcal{S}''_{ij}$, are computed with the depth-averaged eddy viscosity approach. The lateral turbulent mixing coefficient is parameterized as $\nu_t = Nx\sqrt{gD}$ inside the surf zone, where N is the turbulence parameter, and has an exponential decay beyond the breaker line.

Finally, mass conservation of sediment yields the bottom evolution equation,

$$(1-p)\frac{\partial z_b}{\partial t} + \frac{\partial q_i}{\partial x_i} = 0\ , \tag{3}$$

where $p \simeq 0.5$ is the porosity and q_1 and q_2 are the two components of the depth- and wave-averaged volumetric sediment transport ($m^3 m^{-1} s^{-1}$). A general formulation for q_i in the weak current limit is

$$q_i = Q\left(\alpha \mathcal{A}_{ij} v_j - \gamma \frac{\partial z_b}{\partial x_i} + q_i^*\right)\ . \tag{4}$$

Here, Q is a constant, $\alpha(u_w)$ is the wave stirring function, $\mathcal{A}_{ij}(\theta)$ are the components of a second-rank tensor, $\gamma(u_w)$ is the bed-slope coefficient (also depending on the stirring by waves). Finally, q_i^* describes the net sediment transport caused by wave asymmetry and depth-dependent processes that are not explicitly accounted for in the present model; its formulation is discussed later on. The first term on the r.h.s. of Eq. (4) describes the joint effect of waves (stirring sediment from the bed) and currents (causing the transport). The components $\mathcal{A}_{ij}(\theta)$ account for the fact that net sediment can be transported in a direction different than that of the net current (they are called anisotropy tensor components from now on). For instance, Ref. 7 suggests that the direction of measured net transport in the nearshore can deviate up to 15^o from the direction of the net current due to wave effects. The second term in Eq. (4) models the preferred downslope transport of the sand.

Indeed, three well-known transport formulations can be reduced to this form in the weak current limit: Bailard bedload (BB-formula from now on), Bailard suspended load (BS-formula) and Engelund-Hansen total load (EH-formula) [7]. The two Bailard formulas were originally developed for coexistence of waves and currents. On the contrary, the EH-formula was designed for current-dominated conditions and no downslope contribution was supplied. In the present study, however, the total instantaneous current

Table 1. Expressions for Q, α and γ in the four different sediment transport formulations used (Eq. 4). The fraction γ/α is also given. The parameters and their default values are the drag coefficient, $c_d = 0.007$, the reduced gravitational acceleration, $g' = g(\rho_s - \rho)/\rho = 14.7\ \mathrm{ms}^{-2}$, the grain size of the sand, $d = 0.2$ mm, the settling velocity, $w_s = 0.02\ \mathrm{ms}^{-1}$, and the angle of repose of the grains, $\phi = 45^o$.

	Q	α	γ	$\frac{\gamma}{\alpha}$
Engelund-Hansen formula	$\frac{0.04\, c_d^{3/2}}{g'^2\, d}$	$\frac{3}{8}\, u_w^4$	$\frac{16}{15\pi}\, u_w^5$	$\frac{128}{45\pi}\, u_w$
Bailard suspended formula	$\frac{0.01\, c_d}{g'\, w_s}$	$\frac{4}{3\pi}\, u_w^3$	$\frac{0.16}{15\pi\, w_s}\, u_w^5$	$\frac{0.4}{5\pi^2 w_s}\, u_w^2$
Bailard bedload formula	$\frac{0.13\, c_d}{g' \tan\phi}$	$\frac{1}{2}\, u_w^2$	$\frac{4}{3\pi \tan\phi}\, u_w^3$	$\frac{8}{3\pi \tan\phi}\, u_w$

in all the original formulas has been replaced by the depth- and wave-averaged current plus the wave oscillatory contribution and a Bailard-like version for the downslope transport has been added to the EH-formula. After averaging over the wave period, the expressions for Q, α and γ shown in Table 1 are obtained. The anisotropy tensor components, $\mathcal{A}_{ij}(\theta)$, are also different for each formulation, with different dependencies on the angle of wave incidence. However, in case of angles up to 20^o, the expressions can be approximated as

$$\mathcal{A} = \begin{pmatrix} 1+\delta & 0 \\ 0 & 1 \end{pmatrix}, \tag{5}$$

with the values $\delta = 4, 3, 2$ corresponding to the three formulas given in Table 1, respectively.

3. Linear stability analysis

Equations (1), (2) and (3), together with the parameterizations used, define a dynamical system of four equations for the unknowns $\vec{v}$, z_s and z_b. The linear stability approach to the formation of bars by self-organization starts by defining an equilibrium (i.e. steady) and alongshore uniform reference state (without oblique bars). In this study, we assume that the reference profile is planar, $z_b^o(x) = -\beta x$, with β being the slope. The obliquely incident waves generate a longshore current, $\vec{v} = (0, V^o(x))$, and an elevation of the mean free surface, $z_s = z_s^o(x)$. This state represents a morphodynamic equilibrium in case the net cross-shore sediment flux vanishes. This requires the flux q_i^* in Eq. (4) to be

$$q_i^* = \gamma(u_w^o)\frac{\partial z_b^o}{\partial x_i},$$

where u_w^o is the orbital velocity in this equilibrium state. As the parameterizations used are the same as in Ref. 5, the resulting equilibrium state is the analytical solution described in that paper.

Once the reference or basic state has been computed, stability analysis can be applied in a standard way. A small perturbation assumed to be periodic in time and in the alongshore coordinate is added to this basic state,

$$(v_1, v_2, z_s, z_b) = (0, V^o, z_s^o, z_b^o) + \Re e\{e^{i(\kappa y - \omega t)} (u(x), v(x), \eta(x), h(x))\} ,$$

where κ is the alongshore wave number. By inserting these expressions in the governing equations and linearizing with respect to the perturbations, we arrive at an eigenproblem. For each κ, different eigenvalues ω exist, where $\omega = \omega_r + i\omega_i$, and the complex eigenfunctions are $(u(x), v(x), \eta(x), h(x))$. The growth rate of the emerging bedforms is given by ω_i, so that $\omega_i > 0$ means growth and hence an unstable basic state. The migration celerity is $c_m = -\omega_r/\kappa$. The alongshore wavelength of the bars is $2\pi/\kappa$ and their shape is given by $\Re e\{e^{i\kappa y} h(x)\}$. In a similar way, the associated flow and the mean free surface elevation are obtained from $u(x)$, $v(x)$ and $\eta(x)$. In case of an unstable basic state, some perturbations with a positive growth rate are found. The growth rate curves show these positive ω_i for different values of the wave number, κ. The pattern associated to the wave number with the maximum growth rate will initially amplify the fastest and it will determine the initial appearance of the beach.

Out of equilibrium, the dynamics of the cross-shore profiles (2D) is typically slower than the dynamics of the bars we pretend to describe. Therefore, we assume that the perturbations in the wave-driven cross-shore transport q_i^* are negligible in comparison with the perturbations in the transport driven by the depth-averaged circulation. The functions α and γ are not perturbed, either.

4. Results

The present contribution aims at investigating the effect of using the different transport formulas, thereby the model has been only run for the default parameter setting shown in Table 2. The values of the parameters related to the transport formulas have been given in the caption of Table 1. Values for the offshore wave height, H_b, and the surf zone width, X_b, are also shown in Table 2, together with a reference value for the wave orbital velocity, U_w, computed at the breaker line. The angle of wave incidence at the breaker line is the only hydrodynamic parameter that has been varied

Table 2. Default parameter setting used in the study, see the text for details.

Symbol	β	γ_b	c_d	N	θ_b	δ	H_b	X_b	U_w
Value	0.01	0.8	0.007	0.01	10^o	0	0.8 m	100 m	1.25 ms^{-1}

in this study, from 3^o to 20^o. A more detailed description of the results can be found in Ref. 8.

4.1. *Wave stirring*

In the following series of experiments, different cross-shore distributions of the wave stirring function α and the bedslope coefficient γ are used (see Table 1). The anisotropy parameter δ is assumed to be equal to 0, so the transport is isotropic.

Using the EH-formula for the default parameter setting, the results presented in Fig. 1 are obtained. In the figures displayed throughout this paper, the growth rates and migration celerities of the two fastest growing modes are shown for different wave numbers (solid line is the dominant mode, dashed line is the secondary mode). The shape of the topographic perturbation corresponding to these two fastest growing modes is also plotted. In order to visualize the final shape of the beach bottom, the reference sloping profile z_b^0 should be added. In the plots of the topographies, waves approach the coast from the bottom left corner so the induced reference longshore current is directed from left to right (big arrow in the top right corner). Small arrows indicate the main trend in the deviations of the longshore current due to the hydrodynamic circulation induced by the growing bars. The dot-dashed horizontal lines denote the position of the breaker line. In Fig. 1, the growth rate curve of the first mode has a maximum for an alongshore wavelength of $\lambda = 157$ m. The corresponding bottom perturbation grows with a characteristic e-folding time of $T_g = 14$ days and migrates down-flow at 5.6 m per day. The bottom shape consists of alternating shoals and troughs at both sides of the breaker line, with the inner bars having a down-current orientation, i.e. the seaward end of the bars is shifted down-current with respect to their shoreward end. The angle of orientation is about 60^o with respect to the shore normal. This type of topography is called *'crescentic/down-current bars'* from now on. The secondary mode shows no maximum in its growth rate curve, but a representative value for saturation is reached for an alongshore wavelength of $\lambda = 63$ m. It grows in $T_g = 16$ days and migrates down-flow at 0.2 m per day. The bars generated now are only located in the inner surf zone

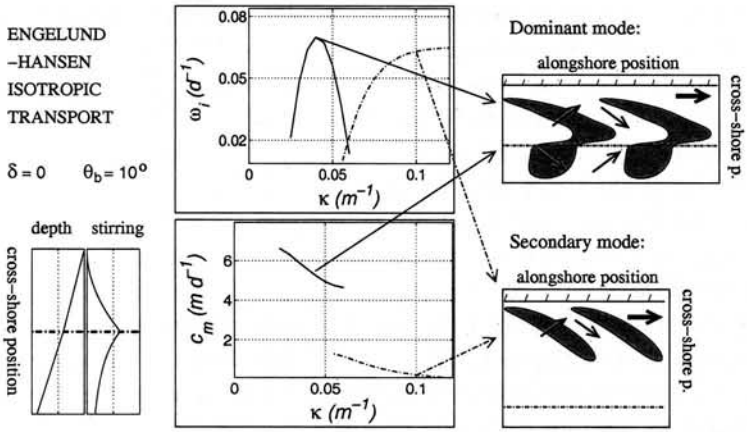

Figure 1. Growth rates, migration celerities and emerging patterns of the two most dominant modes obtained with the EH-formula and the default parameter setting.

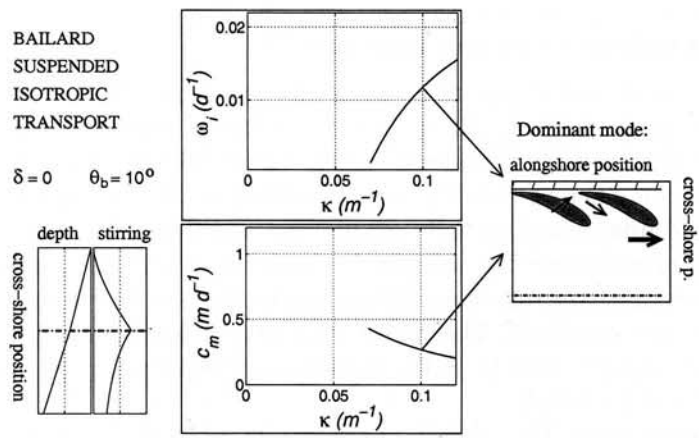

Figure 2. Growth rates, migration celerities and emerging patterns of the two most dominant modes obtained with the BS-formula and the default parameter setting.

and show a down-current orientation, again with an angle of 60° with respect to the shore normal. This type of topography is called *'small-scale down-current bars'*.

Using the BS-formula for the default parameter setting gives the result shown in Fig. 2. Now, the *'small-scale down-current bars'* are the most preferred mode. The growth rate curve has no maximum again and the result is shown for a representative wavelength of $\lambda = 63$ m. Compared

to the previous case the bars now grow with a slower e-folding time of $T_g = 85$ days and migrate down-flow at 0.3 m per day. No secondary modes are obtained, hence the *'crescentic/down-current bars'* obtained before are sensitive to the changes in the cross-shore distribution of the wave stirring. Using the BB-formula no instabilities are found: the growth rates are always negative for all the range of parameter values. In the results for the two first transport formulas, instabilities are only found for $\theta_b < 15°$. The number of growing modes and their growth rate increase when the angle of wave incidence diminishes. The topographic shapes for very small angles can change but the orientation with respect to the current is the same. The main trend of the velocity perturbations induced by the emerging bars in all the solutions is an onshore deflection of the longshore current over the crests and an offshore deflection over the troughs (inside the surf zone). The contrary applies outside the surf zone: offshore deflection over crests, onshore deflection over troughs (see the topographic plots).

4.2. *Anisotropic sediment transport*

Model runs have been performed using the anisotropic versions of the EH-formula and the BS-formula; i.e. by introducing the appropriate values for δ in Eq. (5) ($\delta = 4$ for EH-formula and $\delta = 3$ for BS-formula). The results obtained are different from the ones described in the section above: the number of growing modes, their growth rates and their migration celerities strongly increase and the topographic patterns change significantly. In order to examine the role of anisotropic transport, a smaller value of $\delta = 0.5$ has been also employed. This allows for a better quantitative comparison with the isotropic case ($\delta = 0$), so that an interpretation of these new solutions can be found.

As an example, Fig. 3 displays the results using the BS-formula with the default parameter setting and $\delta = 0.5$. The dominant mode consists of *'down-current bars'* (crossing the breaker line) with a wavelength of 79 m, an e-folding growth time of 2.6 days and a down-flow migration celerity of 10 m per day. The second mode has a spatial pattern that also resembles *'down-current bars'*, but with a more discontinuous shape. The wavelength is 126 m, the growth time 4.2 days and it migrates down-flow at 15 m per day. Comparing these results with those obtained using the isotropic BS-formula (see Fig. 2) shows that the overall orientation of the bars remains the same, but the appearance is quite different. Additionally, the growth rates and migration celerities increase significantly. The main trend of the

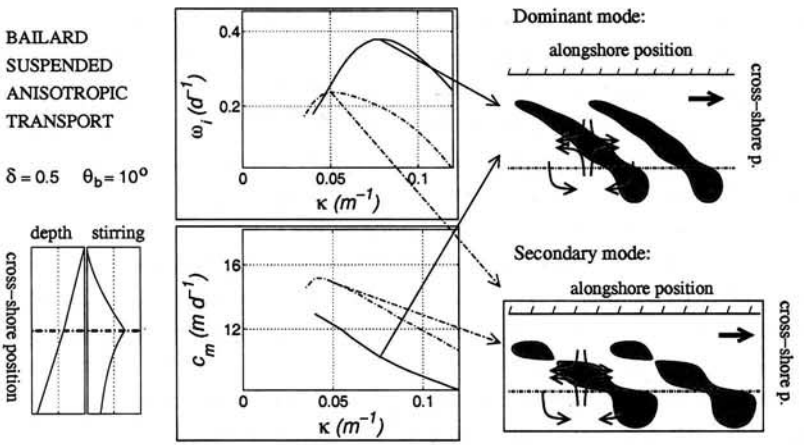

Figure 3. Growth rates, migration celerities and shape of the topography of the two most dominant patterns obtained with the BS-formula using anisotropic transport ($\delta = 0.5$) and the default values for the other parameters.

velocity perturbations in all the solutions obtained in case of anisotropic transport is characterized by the circulation cells plotted over the bars in Fig. 3. These cells always lead to a strong deceleration of the cross-shore component of the velocity in the offshore direction (both inside and outside the surf zone).

5. Discussion and physical mechanism

Firstly, the results obtained for isotropic transport are compared to the solutions presented in Ref. 6. The transport formulation used in that paper (called RF-formula from now on) can also be reduced to Eq. (4), with the following expressions for the functions Q, α and γ,

$$Q = \frac{0.04\, c_d^{3/2}}{g'^2\, d}\ , \quad \alpha = \frac{3}{8} U_w^4 \left(\frac{H}{H_b}\right)^p\ , \quad \gamma = \frac{3}{8} V_{lon}\, U_w^4 \left(\frac{H}{H_b}\right)^p\ .$$

Here, V_{lon} is the maximum value for the equilibrium longshore current ($V_{lon} = 0.4$ ms^{-1} for the default parameter setting) and the exponent p can have the different values: 2, 1.5, 1 and 0. As can be seen, the RF-α with $p = 2$ corresponds to the EH-α inside the surf zone (where $H = \gamma_b D$), as in this region EH-α increases with $u_w^4 \sim H^2$ (see Table 1). However, they differ outside the surf zone (where H = const.), as EH-α decreases with $u_w^4 \sim D^{-2}$ while RF-α remains constant. The two bed-slope coefficients are also slightly different, both their cross-shore distribution and their maximum

value. In particular, the maximum value of the fraction γ/α is 2 times larger in the EH-formula. This fraction determines the importance of the damping mechanism because the downslope transport always causes erosion of the bars. A similar correspondence can be found between the RF-formulation with $p = 1.5$ ($p = 1$) and the BS-formula (BB-formula). Using a value $p = 0$ in the RF-α describes a situation of constant wave stirring along the surf zone, which is not reproduced by the formulas used in the present work.

The topographic patterns for the two fastest growing modes obtained with the EH-formula (Fig. 1) are similar to the ones obtained with the RF-formula with $p = 2$ (described in Ref. 6). More differences are found in the growth rates and migration celerities. In particular, the growth rates of the *'crescentic/down-current bars'* and the *'small-scale down-current bars'* obtained with the EH-formula are 6 and 2 times smaller than using the RF-formula, respectively. The fact that the maximum of the fraction γ/α is 2 times larger in the EH-formula explains why the growth rates are about two times smaller. The growth rates of the *'crescentic/down-current bars'* have an additional decrease by a factor of 3, due to the realistic decrease of α outside the surf zone in the EH-formula. Hence, the specific cross-shore distribution used for the α function, specially outside the surf zone, strongly affects the dynamics of this pattern.

The results obtained with the BS-formula using isotropic transport are also comparable to the ones with the RF-formula using $p = 1.5$. This p value was not used in Ref. 6, but additional runs with the RF-formula have been done. In both cases, the growth rates decrease more than one order of magnitude with respect to the results for the two previous cases (EH-formula and RF-formula using $p = 2$). In general, following the physical mechanism described in Ref. 6 for these solutions, the smaller the exponent of p in α, the weaker the instability. Moreover, the Q in the BS-formula is 10 times smaller than the Q in the EH-formula. These two facts explain why the growth rates are so small. Again, the change in α has a stronger effect in the *'crescentic/down-current bars'* (this mode even disappears for the BS-formula, see Fig. 2) than in the *'small-scale down-current bars'*. Using either the BB-formula or the RF-formula with $p = 1$, no instabilities are found.

Another interesting result of the present work is the strong effect of anisotropic sand transport on the characteristics of the bars. The growth rates increase by a factor of 30 with respect to the isotropic case and the patterns change (compare Fig. 3 with Fig. 2). This indicates that including the anisotropy generates a new physical mechanism that leads to the domi-

nance of different patterns. A convenient way to study this mechanism is to derive an equation from combining conservation of water mass (Eq. 2) and conservation of sediment mass (Eq. 3), and linearizing it with respect to small perturbations superimposed on the equilibrium solution. The result is called Bed Evolution Equation (BEE from now on) and reads

$$\frac{\partial h}{\partial t} + \frac{\alpha V^o}{D^o}\frac{\partial h}{\partial y} = -\alpha\left((1+\delta)u\frac{\partial}{\partial x}\left(\ln\frac{\alpha}{D^o}\right) + \delta\frac{\partial u}{\partial x}\right) . \qquad (6)$$

Here, V^o is the equilibrium longshore current, $D^o = z_s^o - z_b^o$ is the reference water depth, and h and u are the perturbations in the bottom level and in the cross-shore velocity, respectively.

The first term on the l.h.s. of the BEE represents the growth or decay of bedforms. The second term describes the alongshore migration of bedforms with a local celerity $\alpha V^o/D^o$. The downslope transport has not been included in Eq. (6) for the sake of simplicity, as it only causes damping of bed perturbations. Only positive terms on the r.h.s. can initiate growth of the bedforms (i.e., $\partial h/\partial t > 0$ in areas where $h > 0$). The first term in the r.h.s. of the BEE describes the growing mechanism that explains the solutions in the isotropic transport case ($\delta = 0$) and the effect of changing α (see 6 for more details).

When anisotropy is included in the model ($\delta > 0$), a second term appears on the r.h.s. of Eq. (6), related to the cross-shore acceleration of the current ($\partial u/\partial x$). This term is dominant because the scale of the changes in u (given by the cross-shore span of the bars) is quite smaller than the scale of changes in α/D^o (the surf zone width). In order to have growth, a cross-shore deceleration must occur over the bars ($\partial u/\partial x < 0$), which can be observed in all the solutions for the anisotropic transport (see Fig. 3). In order to understand the correlation between $\partial u/\partial x$ and h, the crucial hydrodynamic mechanism is the generation of vorticity by bars and pools (see Ref. 2). Notice that other mechanisms may also be important, for example the bed-flow and bed-surf interactions described in Ref. 6.

6. Conclusions

Two main conclusions arise regarding the sensitivity to the transport formulas. Firstly, the growth rates of the emerging bars depend on the cross-shore distribution of the wave stirring functions, which is different in the three formulations tested. Secondly, the introduction of a small anisotropy affects strongly the characteristics of the bars, both their growth rates and their topographic shapes.

Using the EH-formula two patterns are found: *'crescentic/down-current bars'*, with wavelengths of $1-2$ times the surf zone width and growth times of the order of days and *'small-scale down-current bars'*, with wavelengths of 0.5 times the surf zone width and similar growth times. Using the BS-formula (without anisotropy) only the *'small-scale down-current bars'* emerge and their growth times are of the order of a few months. Hence, the cross-shore distribution of the stirring function strongly affects the results, specially for the patterns with bars at both sides of the breaker line. Using the BB-formula, no instabilities are found. A new kind of bottom mode is found when the directions of the net sediment transport and net currents are different (anisotropic transport). The patterns are mostly *'down-current bars'* of different wavelengths, which grow in a few days. The physical mechanism that causes the emergence of these new bars is related to frictional torques that induce strong vorticity patterns over the bars.

Acknowledgments

Funding of the EU-commission in the framework of the HUMOR research project (contract EVK3-CT-2000-00037) is gratefully acknowledged. The work of N.C. Vis-Star is supported by 'Stichting voor Fundamenteel Onderzoek der Materie' (FOM), which is supported by the 'Nederlandse Organisatie voor Wetenschappelijk Onderzoek' (NWO).

References

1. Christensen, E.D., Deigaard, R. and Fredsoe, J., Sea bed stability on a long straight coast, *Proc.* 24^{th} *Int. Conf. Coastal Eng.*, 1865-1879 (1995).
2. Falqués, A., Montoto, A. and Iranzo, V., Bed-flow instability of the longshore current, *Cont. Shelf Res.* **16(15)**, 1927-1964 (1996).
3. Hino, M., Theory on formation of rip-current and cuspidal coast, *Proc.* 14^{th} *Int. Conf. Coastal Eng.*, 901-919 (1975).
4. Konicki, K.M., and Holman, R.A., The statistics and kinematics of transverse bars on an open coast. *Mar. Geol.* **169**, 69-101 (2000).
5. Longuet-Higgins, M.S., Longshore currents generated by obliquely incident sea waves, *J. Geoph. Res.* **75 (33)**, 6778-6801 (1970).
6. Ribas, F., Falqués, A. and Montoto, A., Nearshore oblique sand bars, *J. Geoph. Res.* **108 (C4)**, 3119, doi:10.1029/2001JC000985 (2003).
7. Soulsby, R., *Dynamics of Marine Sands*, Thomas Telford Publications (1997).
8. Star, N.C., *Modelling the role of waves and currents in the formation of nearshore oblique sandbars*, IMAU report, Utrecht Uni., Netherlands (2004).